ACS APPLIED MATERIALS & INTERFACES

Research Article

www.acsami.org

Polyoxometalate–Reduced Graphene Oxide Hybrid Catalyst: Synthesis, Structure, and Electrochemical Properties

Yong Kim and Sangaraju Shanmugam*

Department of Energy Systems Engineering, Daegu Gyeongbuk Institute of Science and Technology (DGIST), Daegu 711-817, Korea

Supporting Information

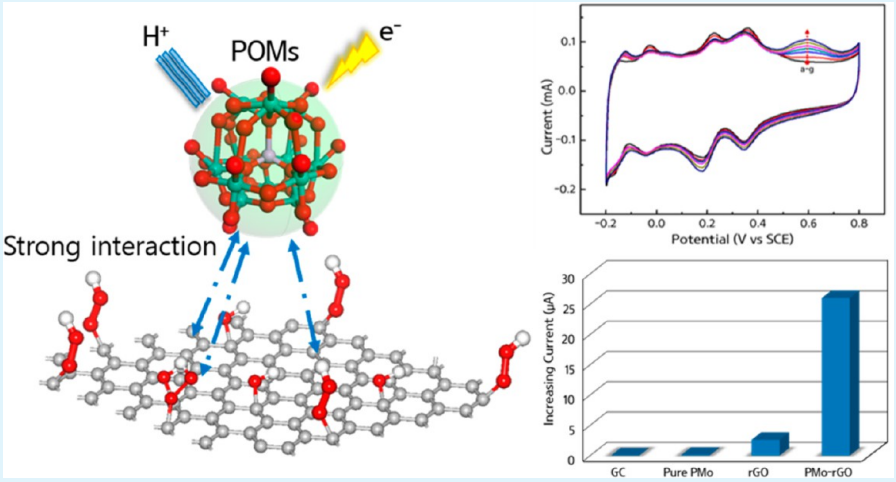

ABSTRACT: The deposition of polyoxometalate (POM) on chemically reduced graphene oxide sheets was carried out through electron transfer interaction and electrostatic interaction between POM and graphene sheets to make a heterogeneous catalyst in aqueous media. Well dispersed individual phosphomolybdic acid (PMo) clusters were observed by electron microscopy and atomic force microscopy measurements. The interaction between polyoxometalate and the graphene sheet was confirmed by using various spectroscopic methods such as FT-IR, UV–vis, and Raman. The UV–visible, IR, and cyclic voltammetry results revealed alteration of the electronic structure of deposited PMo as a result of strong interaction with the graphene oxide surface. Electrochemical properties of the PMo-rGO catalyst were investigated in an aqueous acidic electrolyte. The hybrid catalyst showed enhanced electro-oxidation of nitrite compared with pure homogeneous PMo and rGO.

KEYWORDS: *polyoxometalate, Keggin type, heterogeneous catalyst, reduced graphene oxide, electrochemical activity, nitrite oxidation*

1. INTRODUCTION

Polyoxometalates (POMs) are composed of d-block transitional metal-oxide nanosized, anionic cluster structures and are prospective candidates for electrocatalysis due to their multiple redox properties.[1−5] POMs are well-defined at atomic-molecular levels with a wide range of structures.[4] In particular, the Keggin type POMs ($XM_{12}O_{40}^{n-}$, X = P, Si/M = W, Mo, V), which offer favorable accessibility of electron transfer from empty d orbitals for metal–oxygen π bonding,[2] consist of an encapsulated central XO_4 tetrahedral structure and 3 octahedrals sharing corners, edges, and terminal sites made by 12 pieces of MO_6 octahedral addenda atoms. Keggin polyoxometalates can undergo a stepwise multielectron reversible redox process photochemically, radiolytically, and electrochemically without any structural changes. The redox properties can be easily altered by substitutions in addenda or heteroatoms. Due to their excellent properties, POMs have been exploited in a wide range of electrochemical applications such as photoelectrocatalysts,[6−8] energy conversion and storage systems (fuel cells,[9−11] battery applications,[12,13] pseudocapacitors[14,15]), and sensors[3,16−18]

The electrochemical behavior of POMs in acidic media involves one or two electron reversible reductions to produce reduced POMs, or so-called heteropoly blues owing to their changed color, and further irreversible multielectron reduction with decomposition in the homogeneous state. The reduction reaction can be accompanied by protonation depending on the pK_a, as delineated in the following eqs 1−3 to explain the reduction process with protonations.[19−21]

$$\alpha\text{-}XM_{12}O_{40}^{n-} + 2e^- + 2H^+ \rightarrow \alpha\text{-}H_2XM_{12}O_{40}^{n-} \quad (1)$$

Received: October 2, 2013
Accepted: October 29, 2013
Published: October 29, 2013

$$\alpha\text{-}H_2XM_{12}O_{40}^{n-} + 2e^- + 2H^+ \rightarrow \alpha\text{-}H_4XM_{12}O_{40}^{n-} \quad (2)$$

$$\alpha\text{-}H_4XM_{12}O_{40}^{n-} + 2e^- + 2H^+ \rightarrow \alpha\text{-}H_6XM_{12}O_{40}^{n-} \quad (3)$$

The Keggin type POMs exhibit primary, secondary, and tertiary structures.[4,22] The well dispersed state of POMs on the supports exist mainly in the primary structure, which plays the role of a strong Brönsted acid to ionize protons in an aqueous solution in polyanions.[21] However, the degradation of POMs in aqueous media is a drawback for heterogeneous catalytic activity, despite maintaining good electrochemical activities. Another obstacle for heterogeneous catalyst application is its low surface area owing to its unique cluster structure, and thus good dispersion conditions are required. These significant aspects have prompted researchers to anchor POM on a support material such as silica,[23−26] metal cations (Cs, Co, Fe, etc.),[27−30] positively charged polymer chains,[8,31] and carbon. Entrapping a positively charged polymer matrix on the electrode surface provided strong interaction via electrostatic bonding between the cationic polymer and heteropolyanions but accompanied problems of suitable uniform dispersion of POMs on the electrode, and the insulation effect was not resolved. A common support material is silica, but it is barely suitable for electrochemical studies due to its low conductivity. Many researchers have reported that carbon is an ideal support for anchoring POMs, because POMs have spontaneous interaction with carbon materials. Various carbon-based materials such as activated carbon,[32] carbon nanotubes,[12,33,34] HOPG,[35] glassy carbon,[36] and graphene sheets[7,13,19,37−39] have been used as supports to disperse POMs.

Graphene, consisting of a monolayer of sp^2 carbon atoms, is an attractive material in many research fields including electrocatalytic applications owing to its unique properties such as high surface area, outstanding electrical properties, and high mechanical and thermal properties.[40,41] Graphene is a unique candidate for a POM support material to overcome problems of both low surface area and high solubility of POMs. POM-graphene oxide composites have been fabricated using various reduction methods, such as UV photoreduction,[7,8,19,42] electrochemical reduction,[13] and chemical reduction fabrication methods.[39] However, the strength of the interaction between graphene oxide and POMs has not been addressed in detail. Tessonnier et al. modified a thermally reduced graphene oxide with POMs, enhancing the dispersion via alkyl chain functional groups on the graphene sheet.[38] However, the reported method is complex, and moreover the graphene sheet must be functionalized and the anchoring strength was not studied in detail. In this study we focus on a simple and well-defined fabrication of chemically reduced graphene oxide and Keggin type POMs (Phosphomolybdic acid, PMo). We also optimize the interaction between reduced graphene oxide and PMo by using spectroscopy measurements and morphology analyses to confirm the alteration of original properties of both POMs and the reduced graphene oxide sheet. The reduced graphene oxide prepared by using a hydrazine reduction method partially exhibits unreduced oxygen functional groups, such as hydroxyl and carboxyl groups on the graphene oxide surface. These functional groups are important to maximize the electrostatic interaction between PMo and graphene oxide. This interaction is much stronger than the charge transfer interaction between pristine carbon and POMs and thus can enhance the binding strength between the two constituent materials to yield an immobilized hybrid catalyst. Furthermore, we found that strong hybridization is beneficial for enhancing the electrocatalytic oxidation of nitrite compared to individual bulk PMo or rGO catalysts. The advantage of well dispersed PMo on rGO is that both catalyst activity and stability can be achieved. To the best of our knowledge, there have been no reports on the electrochemical oxidation of nitrite using PMo or a PMo hybrid catalyst.

2. EXPERIMENTAL SECTION

2.1. Preparation of Graphene Oxide. Graphene oxide (GO) was oxidized from graphite powder by a modified Hummer method.[43] One gram of graphite power (Sigma Aldrich) was ground with 50 g of sodium chloride (Daejung, Seoul, Korea) and washed with deionized (DI) water and ethanol 5−10 times to remove sodium chloride. After drying, 4 mL of H_2SO_4 (Sigma Aldrich, 99%) was added and mixed with 0.84 g of $K_2S_2O_8$ (Kanto, Japan) and P_2O_5 (Kanto, Japan) at 80 °C (375 rpm) for 4.5 h. After the mixture cooled for 10−20 min, 167 mL of DI water was added, and the mixture was stirred overnight at room temperature. The mixture was then filtered and washed using DI water and ethanol and subsequently dried for 1 h. The collected powder was added to 40 mL of H_2SO_4 with 5 g of $KMnO_4$ (Aldrich) in a two-neck flask placed in an ice bath and stirred slowly until the contents were completely dissolved. Then, 84 mL of DI water was added into the mixture, which was stirred for 2 h at 35 °C. Finally, more DI water (167 mL) was added along with 10 mL of H_2O_2 (Samchun, Korea), and the reaction was terminated via stirring for 30 min in an ice bath. The resulting mixture was centrifuged until reaching pH 7, and then a brown powder was collected after drying in a vacuum oven.

2.2. Preparation of Reduced Graphene Oxide. Graphene oxide (GO) 1 g was dispersed in 250 mL of DI water for 30 min. Five mL of hydrazine hydrate (Aldrich) was added into the mixture, which was then stirred for 4 h at 100 °C under a nitrogen atmosphere. Finally, the resulting mixture was filtered and washed until reaching pH 7 and then dried at 40 °C for 24 h in a vacuum oven.

2.3. Preparation of PMo-rGO Catalysts. The reduced graphene oxide (rGO, 100 mg) was dispersed and sonicated in DI water for 30 min by using an ultrasonicator. In this step, 1 wt % of ethylene glycol (Aldrich) was added to the graphene solution to disperse POM on the graphene sheet, because POM and the reduced graphene oxide solution can play the role of a Brönsted acid and base, which react with each other by electrostatic interaction. Therefore, ethylene glycol, a diol solvent contributed to an appropriate, mild pH condition for the interaction. An aqueous solution of 20 mg mL^{-1} of phosphomolybdic acid n-hydrate (Kanto, Japan) was added to the rGO solution and mixed for 24 h. Finally, the resulting contents were filtered and washed 3 times with DI water to remove residual physically absorbed POMs on the rGO, followed by drying at 60 °C overnight in a vacuum oven.

2.4. Characterization. Fourier-transform infrared (FT-IR) spectra were obtained on an Agilent Cary 600 FT-IR spectroscope equipped with an autosampler (over 6000 scans) with a resolution of 4 cm^{-1} in a range from 4000 to 400 cm^{-1}. Ultraviolet−visible (UV−vis) spectroscopy was performed with an Agilent Cary-5000 with UV quartz cells. The scanning speed was 400 nm•min^{-1} in the range of 200 to 800 nm. Raman spectroscopy was carried out using an Almega XR (Thermo Scientific) with incident laser light. Atomic force microscopy (AFM) was performed with a NX10 (Park systems) in the noncontact mode. The sample was coated on a glass plate treated with ozone by using a spin coater. Transmission electron microscopy (TEM) was performed with a HF-3300 (Hitachi) with an acceleration voltage of 300 kV. Cyclic voltammetric (CV) measurements were performed with a Biologic potentiostat/galvanic with a three-electrode cell configuration using Pt wire, Ag/AgCl saturated electrode, and glassy carbon (3 mm, ϕ) as counter, reference, and working electrodes, respectively, in 1 M H_2SO_4. The electrode ink was prepared by dispersing 5 mg of a sample in 125 μL of isopropyl alcohol and 125 μL of DI water, and 10 μL of 5 wt % Nafion solution (Aldrich) was added finally. The glassy carbon (GCE) working electrode was polished in a diamond solution and a 0.05 μm Al_2O_3 paste before coating ink on the

surface of the GCE. Then, 3 μL of well dispersed ink was dropped onto the glassy carbon surface and dried at room temperature in order to form a uniform thin film of the catalyst. All CV measurements were recorded using a potential window between −0.2 and 0.8 V at different scan rates. A nitrite oxidation reaction was carried out using different concentrations from 100 μM to 600 μM $NaNO_2$ at a 10 mV s^{-1} scan rate. A long-term electrochemical stability test was performed up to 100 cycles at a 50 mV s^{-1} scan rate under the same conditions.

3. RESULTS AND DISCUSSION

3.1. Morphology Analysis. The TEM image of graphene oxide revealed a crumpled, paper-like morphology (Figure 1a). From TEM studies of PMo-rGO particles with a size range of 1−6 nm were observed on the graphene sheet. The well dispersed state of individual PMo clusters (Figure 1b) suggests that the POMs strongly interacted with the carbon framework of graphene. In particular, larger particles at some regions or edges were observed, and they resulted from aggregation of POMs through strong interactions with oxygen containing functional groups on the graphene sheet, such as hydroxyl and carboxyl groups. The POMs can form three types of crystalline structures, primary, secondary, and tertiary structures. The tertiary structure contains hydronium ions (H_3O^+), which connect neighboring polyoxometalate clusters,[4,38] whose size is greater than ∼2 nm. Schwegler et al. reported that POM clusters interact with oxygen containing functional groups of activated carbon such as hydroxyls, carbonyls, and ether groups.[32] In particular, the carboxyl group is weakly acidic in aqueous media, but when it is mixed with POMs that have a lower pH value, it plays the role of a weak base by changing to a positive charge. As a result, POMs and surface functional groups of graphene can easily interact via electrostatic bonding between positively charged carboxyl groups and negatively charged POM anions in aqueous solvents. Therefore, particle size was attributed to the degree of interaction between functional groups and cluster molecules. Moreover, HR-TEM images (Figure 1c) indicated that the size of single molecules of PMo were around 2−3 nm. The dark spots marked with arrows in Figure 1c are PMo individual clusters well dispersed on the graphene oxide surface.

In order to support our observations, the PMo-rGO sample was further characterized by AFM. PMo-rGO was coated on a glass plate to perform AFM. The glass plate was pretreated in ozone to render the glass plate hydrophilic. The PMo-rGO dispersion was spin-coated on a pretreated glass plate at 1000 rpm for 30 s, and the residual solvent was evaporated at 60 °C. Figure 2 shows an AFM image of PMo-rGO, indicating that the height of individual particles on the graphene sheet is around 1−2 nm. The particle size observed from the AFM results is in good agreement with the TEM observations.

3.2. Characterization of PMo-rGO. Keggin type POMs were immobilized onto several support materials such as positively charged polymer, silica, and carbon material. In particular, interaction between pristine graphene and polyoxometalate is a spontaneous reaction where PMo is strongly adsorbed owing to electron transfer from the electron-abundant polyoxometalate to the graphene sheet.[13,19,38] In order to understand this interaction, FT-IR spectroscopy is usually used to analyze the characteristic vibrational peak shift of the metal-oxide on polyoxometalate. PMo has four types of metal−oxide bonds, a three metal−oxygen sharing structure of MoO_6 octahedra by edge-sharing oxygen atoms (Mo−O_b−Mo), corner-sharing oxygen (Mo−O_c−Mo), central atom-oxygen

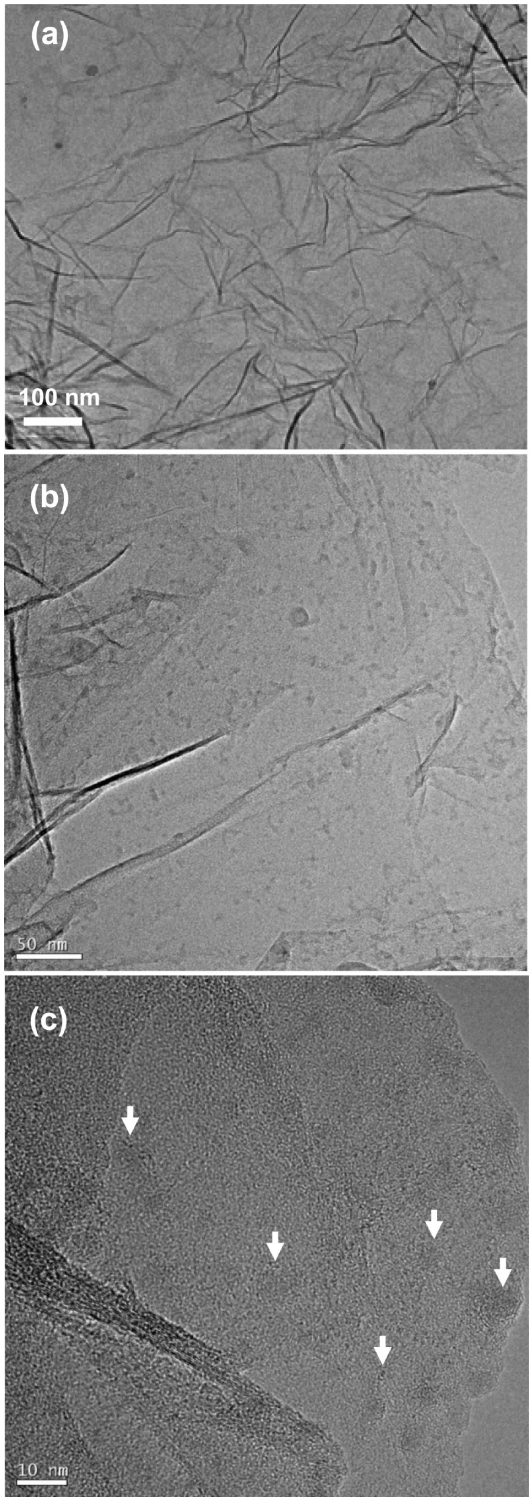

Figure 1. TEM images of (a) rGO and (b, c) PMo-rGO. The arrows indicate individual PMo clusters on the graphene surface.

sharing (P−O) to make a cage, and a terminal metal oxygen (Mo═O_t), which are formed by double bonds.[38]

The FT-IR spectra of GO, rGO, and PMo-rGO showed characteristic individual functional group vibration peaks (Figure 3a). When the GO reduction reaction occurred, the −OH group (3421 cm^{-1}) and C═O (1728 cm^{-1}) symmetry vibration peaks disappeared, but C═C sp^2 species (1580 cm^{-1}) and C−O (1043 cm^{-1}) vibration peaks remained. This

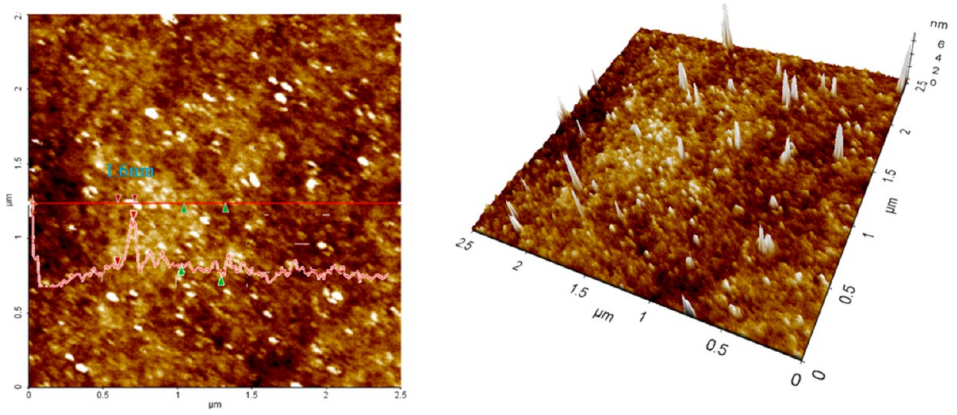

Figure 2. Noncontact AFM image and height profile of PMo-rGO and 3-dimensional image. The dispersed solution of PMo-rGO (0.1 mg mL^{-1}) were coated on the ozone pretreated glass plate by using spin-coating.

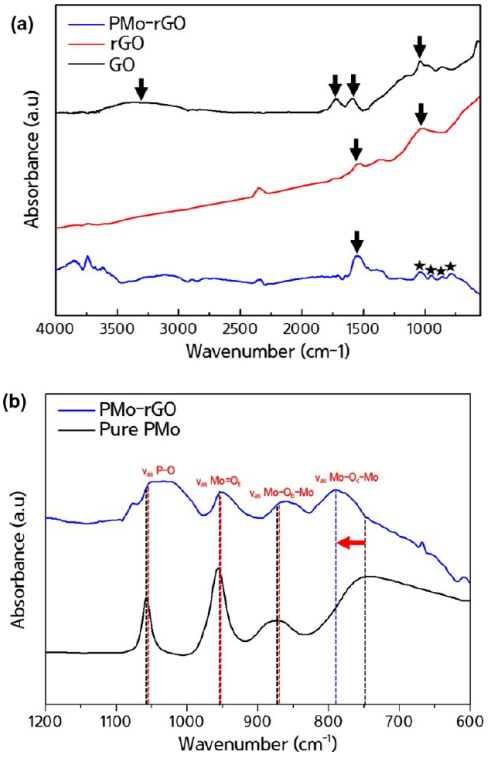

Figure 3. (a) FT-IR spectrum of GO, rGO, PMo-rGO. Each functional group peak and vibration was marked by an arrow, and a star indicated the metal−oxygen vibration peak in the PMo. (b) Peak shift information between pure PMo and PMo-rGO composite. The significant peak shift occurred in the Mo−O_c−Mo, which is marked with a red arrow.

indicates that a partial reduction process occurred by using hydrazine hydrate, which is a mild reducing agent, and thus the reduced graphene oxide obtained by this process exhibits hydrophilic behavior (Scheme 1). This resulted in enhanced interaction between rGO and PMo through electrostatic bonding owing to the remaining oxygen functional group on the graphene sheet. Comparing the rGO and PMo spectra, C=C sp^2 species remained, and M−O stretching at 1035, 948, 861, and 786 cm^{-1} peaks was clearly observed. This implied that PMo was successfully deposited onto the graphene oxide sheet through a simple synthesis method without employing additional procedures.

Scheme 1. Schematic Representation of the Fabrication of PMo-rGO Hybrid Catalyst

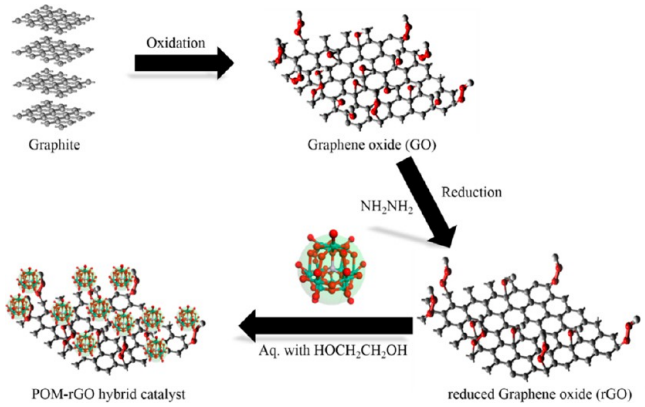

In order to understand the interaction between rGO and PMo, pure PMo and PMo-rGO IR spectra were acquired, and the corresponding results are presented in Figure 3b. The characteristic peak of pure PMo appeared at 1051 cm^{-1} (ν_{as} of P−O), 955 cm^{-1} (ν_{as} of Mo=O_t), 868 cm^{-1} (ν_{as} of Mo−O_b−Mo), and 733 cm^{-1} (ν_{as} of Mo−O_c−Mo). However, the hybrid composite showed peaks at 1035, 950, 866, and 764 cm^{-1} (Figure 3b). A detailed inspection of the peak due to Mo=O_t of PMo-rGo reveals that it is red-shifted from 955 to 950 cm^{-1}, and the band of Mo−O_c−Mo undergoes a blue shift from 733 cm^{-1} to 764 cm^{-1}. This may be ascribed to the interaction between graphene and PMo due to strong adsorption via electron transfer binding and electrostatic binding between them. Notably, the corner-sharing oxygen (ν_{as} Mo−O_c−Mo) vibration shows a much higher peak shift than other octahedral oxygen sharing such as terminal and bridge sharing (around 30 cm^{-1} wavenumber shifted). In the literature, when a POM anion has an effect on the countercation, the Mo−O_c−Mo vibration shifts almost 20 cm^{-1}, depending on the kind of cation.[38,44] This reflects the occurrence of partial protonation, resulting in electrostatic interaction between the POM cluster and the graphene oxide sheet. This observation indicates that the electrostatic interaction contributes more than the electron transfer interaction because of the large amount of oxygen containing functional groups on the graphene oxide surface.

UV−vis spectroscopy was used to measure the ligand-to-metal charge transfer (LMCT) band of the original POMs in the 300−400 nm region. rGO and PMo-rGO samples were

dispersed in ethanol solvent with different concentrations from 0.05 mg mL^{-1} to 0.5 mg mL^{-1}. The pure PMo exhibited a LMCT band at 309.5 nm, as shown in Figure 4a, and this

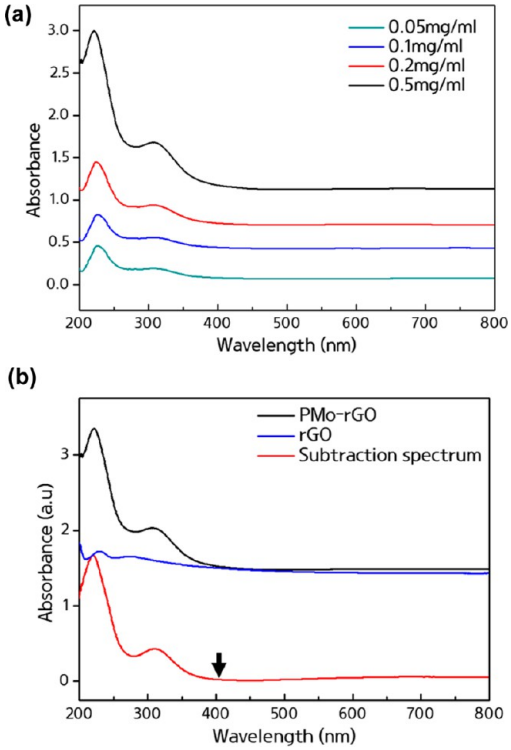

Figure 4. UV−vis spectrum of PMo-rGO. (a) At different concentrations of PMo-rGO dispersion. (b) rGO and PMo-rGO absorbance information and the subtraction spectrum between rGO and PMo-rGO.

observed absorption band value is in agreement with the value reported in the literature.[38] Moreover, subtraction spectra between rGO and PMo-rGO (Figure 4b) were acquired in order to calculate the band gap of PMo-rGO more accurately for comparison between pure PMo and PMo-rGO, which interact with the graphene oxide sheet by transferring an electron from the POM to graphene oxide. The absorption edge wavelength was determined accurately using the first derivative curve of the subtracted spectra between rGO and PMo-rGO, as shown in Figure S1. Pure PMo has a band gap of 2.59 eV[38] (edge wavelength 480 nm), and the PMo-rGO exhibited a band gap of 2.75 eV (edge wavelength 451 nm). The shift in the band gap of the PMo-rGO hybrid clearly shows the changed energy levels of PMo due to electron transfer from PMo to reduced graphene oxide. The electron transfer and electrostatic interaction between PMo and rGO were supported by UV−vis and FT-IR results.

The significance of the interaction between rGO and PMo-rGO can be analyzed by the changes of the carbon framework using Raman spectroscopy. UV−vis spectra showed an electron transfer interaction between PMo and rGO from the value of the edge wavenumber. In order to further confirm this interaction, the structural information of graphene oxide including defects and disorder properties was examined by Raman spectroscopy. The band at 1396 cm^{-1} (D) is attributed to the amount of defects existing in the carbon framework, and the band at 1675 cm^{-1} (G) corresponds to the E2g mode of hexagonal sp^2 carbon domains, representing the degree of graphitization (Figure 5). The intensity ratio between the D and G bands (I_D/I_G ratio) indicates the degree of defects,

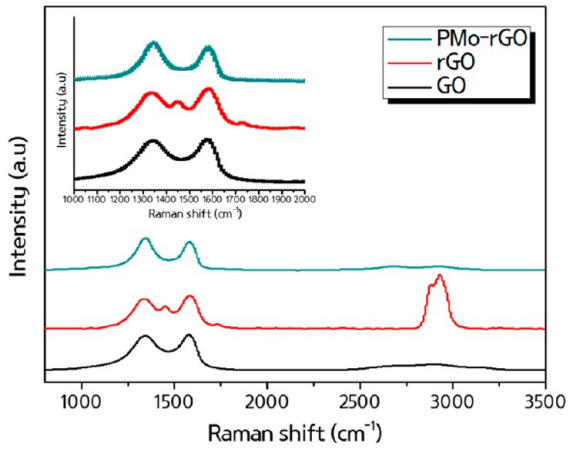

Figure 5. Raman spectra of GO, rGO, and PMo-rGO. The inset shows the expanded region from 1100 to 2000 cm^{-1}.

ripples, edge, and the average size of sp^2 domains. The measured I_D/I_G ratio for GO and rGO was found to be 0.96 and 0.97, respectively. The ratio increased from GO to PMo-rGO, after PMO deposition on rGO, the I_D/I_G ratio was 1.02. This indicated that deposition of POMs results in increased defects, disorder, and sp^2 domain sites on the graphene sheet[45] owing to electron movement from the POM oxide to pristine graphene. IR, UV−vis, and Raman data support the interaction between PMo and the graphene sheet, and two kinds of interactions, electron transfer interaction and electrostatic interaction via oxygen functional groups on the graphene sheet, are believed to occur.

3.3. Electrochemical Activities. The electrochemical properties of bulk PMo dissolved in 1 M H_2SO_4 using a glassy carbon electrode was carried out by cyclic voltammetry. The parent PMo exhibits three reversible redox potentials (0.521, 0.350, 0.205 V vs SCE) in acidic media (Figure S2), and each redox potential is attributed to two electron transfer reactions. Figure 6a shows the cyclic voltammogram of the PMo-rGO hybrid electrode in a potential range of −0.2 to 0.8 V at a 10 mV/s scan rate. The CV showed three distinctive reversible redox potentials of 0.354, 0.187, and 0.041 V vs SCE; each peak separation between the anodic and cathodic peaks (ΔE_p) from the first redox peak to third redox peak was 13, 41, an 17 mV, respectively, indicating that each redox reaction corresponded to a two electron process, as delineated in eqs 1−3 earlier.

All peak potentials were shifted to more negative values when PMo was dispersed on rGO, as compared to the potential of the parent PMo. A 200 mV negative shift was observed for all three peaks compared with pure PMo. This shift might be due to stabilization of the energy levels of PMo upon dispersion on rGO, which can be attributed to strong interaction with the graphene oxide surface. A large negative shift of the peak potentials of PMo in PMo-rGO implies that a charge transfer interaction between the carbon framework of graphene and polyoxometalate takes place, which decreases the electron density on the heteropolyanions.[38] This was further corroborated by UV−vis data, which showed a shift in the band gap of PMO-rGO. Thus, the PMo-rGO hybrid catalyst has a strong interaction by charge transfer with graphene oxide accompanied by good dispersion of individual cluster molecules resulting

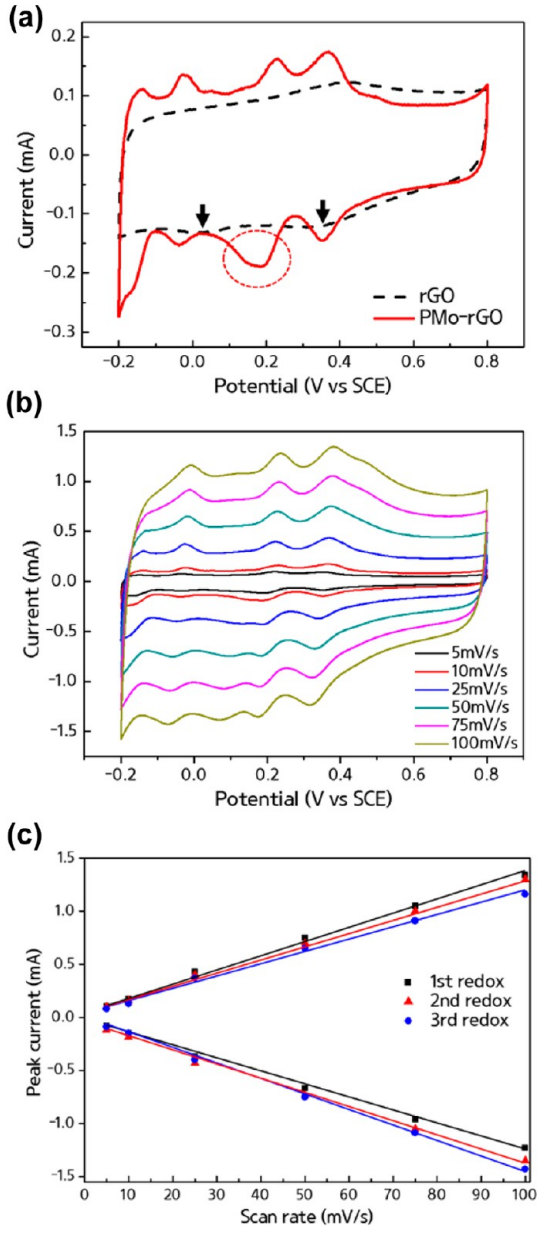

Figure 6. Cyclic voltammetry of PMo-rGO. (a) The comparison CV between rGO and PMo-rGO at a scan rate of 10 mV s^{-1} in 1 M H_2SO_4 electrolyte, the arrows indicate reversible and irreversible redox peak information of rGO, and the red dotted circle indicates the second reduction peak shift and broadening of PMo-rGO. (b) The different scan rate information of PMo-rGO from 5 mV s^{-1} to 100 mV s^{-1}, and (c) the redox peak current versus the scan rate plot.

from a negative shift in electrochemical activity. Moreover, it was observed that there is a PMo-support interaction that resulted in broadening of the second reduction peak, which is highlighted with red dotted circles in Figure 6a. This observed phenomenon can be attributed to reduced graphene oxide electrochemical activity, which was characterized by one reversible redox peak and one irreversible reduction peak at 0.324, 0.02 V vs SCE (black arrows in Figure 6a).

Figure 6b presents the CVs of PMo-rGO at different scan rates (from 5 to 100 mV/s). The anodic and cathodic peak currents increased with an increasing scan rate. The peak separation potential values gradually increased with increasing scan rates. Figure 6c shows the plot of the cathodic and anodic current is proportional to the scan rate; as the scan rate increases, both the anodic and cathodic peak currents increased linearly. This indicated that the electrochemical redox process is a surface dominated electron transfer phenomenon of the PMo-rGO hybrid catalyst. This is further corroborated by rotating disc experiments, where increasing the rotation speed (400, 625, 900, 1225, 1600, 2025 rpm) had no effect on the peak currents (data not shown). These results clearly demonstrate that the charge transfer process in PMo-rGO is a surface phenomenon.

POM modified electrode films are usually unstable when applied in aqueous media during electrochemical activity, because the POMs can easily leach out from the support into the electrolyte, resulting in a decay of current. In order to evaluate the electrochemical stability of the PMo-rGO hybrid electrode, a continuous cycling test was performed with a scan rate of 50 mV s^{-1} for 100 cycles (Figures 7a and 7b). The decay

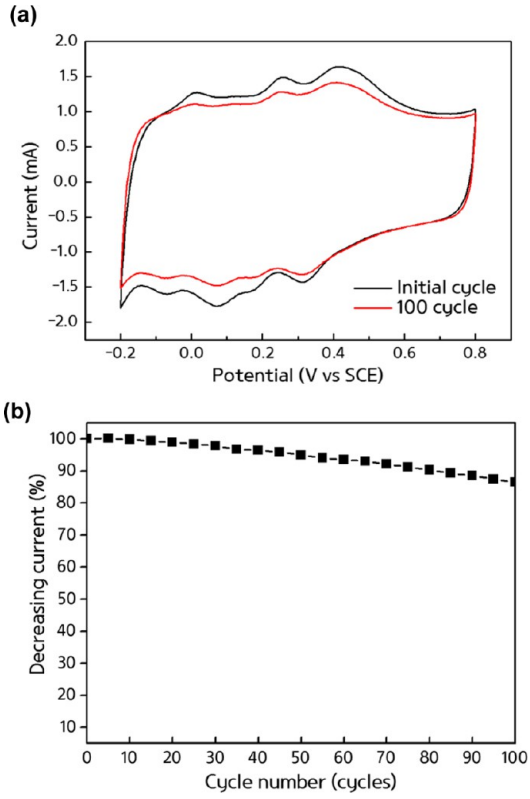

Figure 7. (a) The CV stability test of PMo-rGO for 100 cycles at a scan rate of 50 mV s^{-1} in 1 M H_2SO_4 electrolyte. (b) The current decay of the first reduction peak with the cycle number.

of the first reduction peak current was found to 14.5%, indicating a reasonable electrochemical stability of the hybrid composite due to the strong interaction between the surface functional groups of rGO and PMo.

3.4. Electrochemical Oxidation of Nitrite Ions. Nitrite is highly toxic due to the formation of carcinogenic N-nitrosoamines by reacting with dietary components in the stomach. Thus, the determination or detection of nitrite is an important process.[46,47] In general, nitrite can be determined electrochemically by both oxidation and reduction reactions. The electrochemical reduction of nitrite yields several products depending on the type of electrode and the catalyst used, but an oxidation reaction is a simple straightforward reaction to make

nitrate ions as a final product.[48] POM is well-known for the electrochemical reduction of nitrite ion to ammonia, involving six electrons and eight proton changes in an acid electrolyte.[49,50] However, electrochemical oxidation of nitrite ions by using POMs or POM composite materials has not been explored. In contrast, the electrochemical oxidation of nitrite has been carried out using various materials, such as an Al_2O_3−Pd modified electrode,[51] Au nanoparticles,[47,52] graphene,[48] and glassy carbon.[53] In this work, we identified new electrochemical oxidation properties of a PMo-rGO catalyst; when PMo is hybridized with rGO, improved electrochemical oxidation of nitrite was observed. Previous reports on nitrite oxidation reactions with reduced graphene oxide stated that an oxidation peak appeared at 0.82 V vs SCE in 0.1 M PBS solution (pH 5).[48] However, all previous studies used high concentrations of nitrite ions over 1 mM, and no comparable investigation was carried out using a very low concentration of nitrite ions.

Figure 8a shows the nitrite oxidation reaction of rGO in the 1 M H_2SO_4 electrolyte in a range of −0.2 to 0.8 V under a 10 mV s^{-1} scan rate in the presence of different concentrations of $NaNO_2$ from 100 to 600 μM. The oxidation peak potential was found at 0.61 V vs SCE of the rGO electrode, and the rGO electrode showed an increased peak current of 4.6 μA with the addition of 600 μM of NO_2^-, whereas the PMo-rGO electrode presented a much higher peak current of around 45 μA (Figure 8b), as clearly seen in Figure 8c. For comparison, the nitrite oxidation reaction was carried out on glassy carbon and pure PMo electrodes with the same concentration of nitrite, and the results are shown in Figure S3. No obvious oxidation peak was observed on the GC and PMo electrodes in the same potential window, indicating that these two electrodes are inactive for nitrite oxidation. In order to evaluate the catalytic behavior more quantitatively, the electrochemical catalytic efficiency of electro-oxidation was expressed as[44]

$$\{(I_{(\text{PMo-rGO}+\text{NO}_2^-)} - I_{\text{d(PMo-rGO)}})/I_{\text{d(PMo-rGO)}}\}*100 \quad (4)$$

where $I_{\text{PMo-rGO}+\text{NO}_2^-}$ is the current response of the nitrite ion oxidation peak, where we applied a NO_2^- concentration of 300 μM and $I_{\text{d(PMo-rGO)}}$ is the diffusion current response without nitrite ions. From this equation, PMo-rGO catalyst nitrite oxidation activity was 75%, whereas pure rGO activity was obtained at 3.7%, thus over 20 times improvement of oxidation activity was observed. The sensitivity of the PMo-rGO electrode response for nitrite species within the concentration range is 7.3×10^{-2} A·M^{-1}, while the rGO sensitivity is 7.6×10^{-3}A·M^{-1}, respectively, indicating more than 10-fold enhancement of electrocatalytic sensitivity resulting from the hybridization between rGO and PMo. The possible interferences for the detection of nitrite ion on PMo-rGO electrode was carried out by adding an amount of NO_3^- or H_2O_2 containing 600 μM nitrite. The results indicated that NO_3^- and H_2O_2 had no effect on the NO_2^- oxidation current (Figure S4). The oxidation reaction of nitrite followed by a two-step reaction is expressed as follows:[54]

$$NO_2^- \rightarrow NO_2\cdot + e^- \quad (5)$$

$$2NO_2\cdot + H_2O \rightarrow NO_2^- + NO_3^- + 2H^+ \quad (6)$$

The preceding equations show that an oxidation reaction occurs when one electron transfers and reacts with water molecules to make a nitrate ion and two protons. PMo assisted the oxidation reaction of the graphene sheet by the high electronegativity of metal−oxygen and the production of defect sites on the graphene sheet from well dispersed fabrication with an aqueous solution.

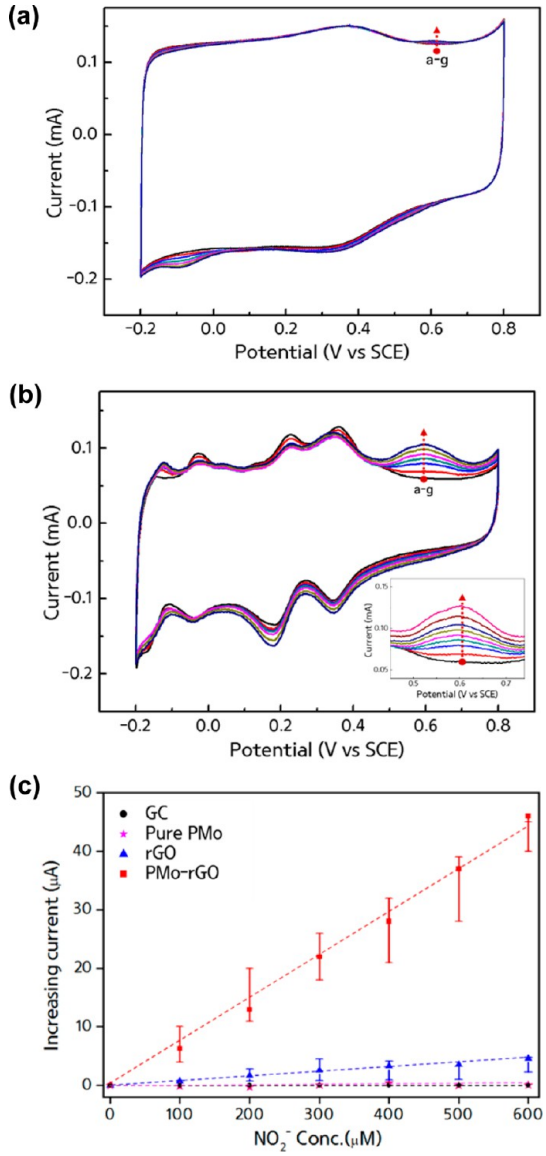

Figure 8. Cyclic voltammetry of (a) rGO and (b) PMo-rGO for nitrite ion oxidation at a scan rate of 10 mV s^{-1} in 1 M H_2SO_4 containing different concentrations of $NaNO_2$ (0, 100, 200, 300, 400, 500, 600 μM of $NaNO_2$ for a−g). (c) The effect of the concentration of NO_2^- on the oxidation peak current of various catalysts.

CONCLUSIONS

We have successfully fabricated a hybrid composite of rGO and PMo through a simple fabrication method in an aqueous solution. Two kinds of interactions are proposed, electron transfer and electrostatic interaction between rGO and POMs, allowing high dispersion of individual clusters of POMs, and strong absorption prevents leaching out into the solvent, as confirmed via FT-IR, UV−vis, and Raman spectroscopy. FT-IR spectra showed electrostatic interaction between the corner shared metal oxygen site of POMs and the oxygen functional group on the graphene sheet. The UV−vis and Raman spectra revealed a strong interaction between the graphene sheet and POMs via electron transfer interaction induced at the defect

site on the graphene sheet, which altered the band gap energy. The electrochemical results of the PMo-rGO hybrid exhibit reversible redox properties and high stability on the aqueous solution. These results indicate that the PMo-rGO hybrid catalyst can be used in heterogeneous catalytic applications, and we investigated and observed high electrocatalytic nitrite oxidation activity over the composite. Based on our results, a wide range of hybrid materials can be prepared using different types of polyoxometalates, and such hybrid materials have potential applications in catalysis, sensors, and related fields.

■ ASSOCIATED CONTENT

Ⓢ Supporting Information

The band gap calculation, CV of pure PMo, nitrite oxidation on GC, PMo, and interference study. This material is available free of charge via the Internet at http://pubs.acs.org.

■ AUTHOR INFORMATION

Corresponding Author

*Phone: +82-53-785-6413. E-mail: sangarajus@dgist.ac.kr.

Notes

The authors declare no competing financial interests.

■ ACKNOWLEDGMENTS

This work was supported by the DGIST R&D Program of the Ministry of Education, Science and Technology of Korea (13-BD-01).

■ REFERENCES

(1) Katsoulis, D. E. *Chem. Rev.* **1998**, *98*, 359−387.
(2) Pope, M. T.; Muller, A. *Angew. Chem., Int. Ed.* **1991**, *30*, 34−48.
(3) Ammam, M. *J. Mater. Chem. A* **2013**, *1*, 6291−6312.
(4) Mizuno, N.; Misono, M. *Chem. Rev.* **1998**, *98*, 199−217.
(5) Poblet, J. M.; López, X.; Bo, C. *Chem. Soc. Rev.* **2003**, *32*, 297−308.
(6) Moon, G.; Park, Y.; Kim, W.; Choi, W. *Carbon* **2011**, *49*, 3454−3462.
(7) Li, H.; Pang, S.; Feng, X.; Müllen, K.; Bubeck, C. *Chem. Commun.* **2010**, *46*, 6243−5.
(8) Li, H.; Pang, S.; Wu, S.; Feng, X.; Müllen, K.; Bubeck, C. *J. Am. Chem. Soc.* **2011**, *133*, 9423−9429.
(9) Choi, S. M.; Seo, M. H.; Kim, H. J.; Lim, E. J.; Kim, W. B. *Int. J. Hydrogen Energy* **2010**, *35*, 6853−6862.
(10) Stanis, R. J.; Kuo, M.-C.; Rickett, A. J.; Turner, J. A.; Herringa, A. M. *Electrochim. Acta* **2008**, *53*, 8277−8286.
(11) Liu, R.; Li, S.; Yu, X. *J. Mater. Chem.* **2012**, *22*, 3319−3322.
(12) Kawasaki, N.; Wang, H.; Nakanishi, R.; Hamanaka, S.; Kitaura, R.; Shinohara, H.; Yokoyama, T.; Yoshikawa, H.; Awaga, K. *Angew. Chem., Int. Ed.* **2011**, *50*, 3471−3474.
(13) Wang, S.; Li, H.; Li, S.; Liu, F.; Wu, D.; Feng, X.; Wu, L. *Chem.—Eur. J.* **2013**, *19*, 10895−10902.
(14) Cuentas-Gallegos, A. K.; Lira-Cantú, M.; Casañ-Pastor, N.; Gómez-Romero, P. *Adv. Funct. Mater.* **2005**, *15*, 1125−1133.
(15) Cui, Z.; Guo, C. X.; Yuan, W.; Li, C. M. *Phys. Chem. Chem. Phys.* **2012**, *14*, 12823−12828.
(16) Haghighi, B.; Hamidi, H.; Gorton, L. *Electrochim. Acta* **2010**, *55*, 4750−4757.
(17) Liu, R.; Li, S.; Yu, X.; Zhang, G.; Zhang, S.; Yao, J.; Keita, B.; Nadjo, L.; Zhi, L. *Small* **2012**, *8*, 1398−1406.
(18) Zhang, H.; Xie, A.; Shen, Y.; Qiu, L.; Tian, X. *Phys. Chem. Chem. Phys.* **2012**, *14*, 12757−12763.
(19) Chen, J.; Liu, S.; Feng, W.; Zhang, G.; Yang, F. *Phys. Chem. Chem. Phys.* **2013**, *15*, 5664−5669.
(20) Gómez-Romero, P.; Nieves, C.-P. *J. Phys. Chem.* **1996**, *100*, 12448−12454.
(21) Sadakane, M.; Steckhan, E. *Chem. Rev.* **1998**, *98*, 219−237.
(22) Kozhevnikov, I. V. *Chem. Rev.* **1998**, *98*, 171−198.
(23) Polarz, S.; Smarsly, B.; Göltner, C.; Antonietti, M. *Adv. Mater.* **2000**, *12*, 1503−1507.
(24) Johnson, B. S.; Stein, A. *Inorg. Chem.* **2001**, *40*, 801−808.
(25) Qi, W.; Li, H.; Wu, L. *J. Phys. Chem. B* **2008**, *112*, 8257−8263.
(26) Grinenval, E.; Rozanska, X.; Baudouin, A.; Berrier, E.; Delbecq, F.; Sautet, P.; Basset, J.-M.; Lefebvre, F. *J. Phys. Chem. C* **2010**, *114*, 19024−19034.
(27) Fukaya, K.; Yamase, T. *Angew. Chem., Int. Ed.* **2003**, *42*, 654−658.
(28) Belai, N.; Pope, M. T. *Chem. Commun.* **2005**, 5760−5762.
(29) Kholdeeva, O. A.; Vanina, M. P.; Timofeeva, M. N.; Maksimovskaya, R. I.; Trubitsina, T. A.; Melgunov, M. S.; Burgina, E. B.; Mrowiec-Bialon, J.; Jarzebski, A. B.; Hill, C. L. *J. Catal.* **2004**, *226*, 363−371.
(30) Le Magueres, P.; Ouahab, L.; Golhen, S.; Grandjean, D.; Peña, O.; Jegaden, J.-C.; Gomez-Garcia, C. J.; Delhaès, P. *Inorg. Chem.* **1994**, *33*, 5180−5187.
(31) Suppes, G. M.; Deore, B. A.; Freund, M. S. *Langmuir* **2008**, *24*, 1064−1069.
(32) Schwegler, M. A.; Vinke, P.; van der Eijk, M.; van Bekkum, H. *Appl. Catal., A* **1992**, *80*, 41−57.
(33) Toma, F. M.; Sartorel, A.; Iurlo, M.; Carraro, M.; Parisse, P.; Maccato, C.; Rapino, S.; Gonzalez, B. R.; Amenitsch, H.; Da Ros, T.; Casalis, L.; Goldoni, A.; Marcaccio, M.; Scorrano, G.; Scoles, G.; Paolucci, F.; Prato, M.; Bonchio, M. *Nat. Chem.* **2010**, *2*, 826−831.
(34) Cuentas-Gallegos, A. K.; Martínez-Rosales, R.; Baibarac, M.; Gómez-Romero, P.; Rincón, M. E. *Electrochem. Commun.* **2007**, *9*, 2088−2092.
(35) Song, I. K.; Kaba, M. S.; Coulston, G.; Kourtakis, K.; Barteau, M. A. *Chem. Mater.* **1996**, *8*, 2352−2358.
(36) Kuhn, A.; Mano, N.; Vidal, C. *J. Electroanal. Chem.* **1999**, *462*, 187−194.
(37) Sloan, J.; Liu, Z.; Suenaga, K.; Wilson, N. R.; Pandey, P. A.; Perkins, L. M.; Rourke, J. P.; Shannon, I. J. *Nano Lett.* **2010**, *10*, 4600−4606.
(38) Tessonnier, J.-P.; Goubert-Renaudin, S.; Alia, S.; Yan, Y.; Barteau, M. A. *Langmuir* **2013**, *29*, 393−402.
(39) Zhou, D.; Han, B.-H. *Adv. Funct. Mater.* **2010**, *20*, 2717−2722.
(40) Moon, I. K.; Lee, J.; Ruoff, R. S.; Lee, H. *Nat. Commun.* **2010**, *1*, 73.
(41) Dreyer, D. R.; Park, S.; Bielawski, C. W.; Ruoff, R. S. *Chem. Soc. Rev.* **2010**, *39*, 228−240.
(42) Cao, L.; Sun, H.; Li, J.; Lu, L. *Anal. Methods* **2011**, *3*, 1587−1594.
(43) Hummers, W. S. J.; Offeman, R. E. *J. Am. Chem. Soc.* **1957**, *80*, 1339.
(44) Shanmugam, S.; Viswanathan, B.; Varadarajan, T. K. *Indian J. Chem.* **2005**, *44*, 994−1000.
(45) Kudin, K. N.; Ozbas, B.; Schniepp, H. C.; Prud'homme, R. K.; Aksay, I. A.; Car, R. *Nano Lett.* **2008**, *8*, 36−41.
(46) Kozub, B. R.; Rees, N. V.; Compton, R. G. *Sens. Actuators, B* **2010**, *143*, 539−546.
(47) Yu, C.; Guo, J.; Gu, H. *Electroanalysis* **2010**, *22*, 1005−1011.
(48) Mani, V.; Periasamy, A. P.; Chen, S.-M. *Electrochem. Commun.* **2012**, *17*, 75−78.
(49) Wang, X.; Kang, Z.; Wang, E.; Hu, C. *J. Electroanal. Chem.* **2002**, *523*, 142−149.
(50) Liang, Y.; He, P.; Ma, Y.; Zhou, Y.; Pei, C.; Li, X. *Electrochem. Commun.* **2009**, *11*, 1018−1021.
(51) Pournaghi-Azar, M.; Dastangoo, H. *J. Electroanal. Chem.* **2004**, *567*, 211−218.
(52) Afkhami, A.; Soltani-Felehgari, F.; Madrakian, T.; Ghaedi, H. *Biosens. Bioelectron.* **2013**, *51*, 379−385.
(53) Wang, Y.; Laborda, E.; Compton, R. G. *J. Electroanal. Chem.* **2012**, *670*, 56−61.
(54) Chen, L. H.; Zang, J. B.; Wang, Y. H.; Bian, L. Y. *Electrochim. Acta* **2008**, *53*, 3442−3445.